Appl. Phys. A (2016) 122:790
DOI 10.1007/s00339-016-0327-x

Applied Physics A
Materials Science & Processing

Electronic excitation and relaxation processes of oxygen vacancies in YSZ and their involvement in photoluminescence

Takaaki Morimoto[1] · Yasuhiro Kuroda[1] · Yoshimichi Ohki[1,2]

Received: 28 February 2016 / Accepted: 28 July 2016 / Published online: 5 August 2016

Abstract Yttria-stabilized zirconia (YSZ) consists of zirconia and yttria and oxygen vacancies appear in accordance with the ratio of yttria. The oxygen vacancy would sometimes give annoyance, but it would be beneficial on other occasions, depending on its applications. Photoluminescence (PL) due to oxygen vacancies induced by photons with energies around 5.5 eV exhibits two decay time constants. As a possible reason for this, an oxygen vacancy changes its charging state from neutral to positive monovalent by losing an electron when YSZ is irradiated by ultraviolet photons. The PL decays either in a ms range or in a ns range, depending on whether the oxygen vacancies are neutral or positive monovalent.

1 Introduction

Yttria-stabilized zirconia (YSZ) is a mixed crystal consisting of zirconia and yttria, in which yttria was added for the purpose of stabilizing unstable zirconia. Various properties of zirconia such as mechanical strength and thermal stability are improved significantly by the addition of yttria. When Zr^{4+} in zirconia is replaced partially by Y^{3+}, oxygen vacancies appear according to the following equation [1, 2]:

$$(1-x)ZrO_2 + (x/2)Y_2O_3 \rightarrow Zr_{1-x}Y_xO_{2-x/2}. \quad (1)$$

Namely, oxygen vacancies are induced with a ratio of $x/2$ by the addition of yttria. In other words, oxygen vacancies in YSZ exist as a part of its crystal structure. This existence form of oxygen vacancies in YSZ is quite different from many other inorganic solid crystals such as silicon dioxide, yttrium aluminate, and lanthanum aluminate, in which oxygen vacancies exist in the form of a point defect.

Due to the presence of oxygen vacancies [3], YSZ, of a film shape with a thickness from around one to tens of micrometers [4, 5], can be a good ionic conductor at high temperatures suitable as a solid electrolyte in solid oxide fuel cells (SOFCs). On the other hand, YSZ has low electron conductivity and high relative permittivity of about 27 at room temperature. By this nature, it is expected as a high-permittivity material for a gate insulator in a metal–oxide semiconductor (MOS) transistor, which can replace silicon dioxide used for many years [6]. For this application, the thickness of YSZ is in a range from 1 to 10 nm for advanced MOS field-effect transistors (FETs) for large-scale integrated circuits (LSIs) or in a range from 0.1 to 1 μm for power MOSFETs [7, 8].

In general, if point defects are present in an insulator, localized electronic states are formed inside its forbidden band, which can cause a leakage current if the insulator is used as a gate dielectric in a semiconductor device. On the other hand, they provide paths of ionic transport in the case of YSZ when it is used as a solid electrolyte in a SOFC [3–5]. The authors have demonstrated that photoluminescence (PL) and its decay profile provide a good tool to examine the behavior of various point defects in many oxides [9–26]. As for YSZ, its oxygen vacancy has at least

✉ Takaaki Morimoto
takaaki.morimoto@aoni.waseda.jp

✉ Yoshimichi Ohki
yohki@waseda.jp

[1] Department of Electrical Engineering and Bioscience, Waseda University, Shinjuku, Tokyo 169-8555, Japan

[2] Research Institute for Materials Science and Technology, Waseda University, Shinjuku, Tokyo 169-8555, Japan

two charging states, namely neutral and positive monovalent [24]. However, neither the processes by which two types of oxygen vacancies are induced nor their excitation and relaxation processes are clear. Therefore, the subject of this research is to clarify these processes by measuring electron spin resonance (ESR) spectra and the temperature dependence of PL decay.

2 Experimental procedures

Film samples of YSZ were prepared by the following method: First, three kinds of YSZ solutions, which, respectively, contain 10, 15, and 20 mol% of yttria, were made by mixing an alkoxide solution containing 5 wt% of Zr (density 0.90 g/cm^3) and another one containing 3 wt% of Y (density 0.92 g/cm^3), both purchased from Kojundo Chemical Laboratory. A silica glass plate with a thickness of 0.5 mm was used as a substrate. While the substrate was rotating at a speed of 500 rpm, a drop of one of the above YSZ solutions was dropped and spin-coated on it for 10 s first and then at 2000 rpm for the next 20 s. Then, each coated substrate was annealed at a temperature of 300, 500, or 800 °C for 2 h in oxygen. By this process, a YSZ thin film was obtained. Its thickness was about 54 nm as will be mentioned later. On the other hand, thick films are suitable to measure optical absorption and PL spectra clearly. Therefore, for those measurements, the above-mentioned spin-coating was repeated three times to obtain films about 160 nm thick. In addition to the film samples, commercially available YSZ (100) single crystal with an yttria/zirconia ratio of 9.8:90.2 in mol%, which had been grown with the skull-melting method by Crystal Base Co. and had been cut to rectangular plates with a thickness of 0.5 mm, was used.

The plate and film samples were analyzed by the following procedures in order to examine electronic excitation and relaxation processes of oxygen vacancies: First, in-plane X-ray diffraction (XRD) patterns were obtained with Cu Kα X-rays at room temperature using Rigaku Rint-Ultima III. Next, optical absorption spectra in a visible–ultraviolet (Vis–UV) range from 2.0 to 6.5 eV were obtained with a double-beam spectrophotometer (Shimadzu UV-3100PC) in a transmission mode at room temperature.

Furthermore, PL spectra and PL decay curves in a ms range were measured at temperatures from 77 to 270 K with a fluorescence spectrometer (JASCO FP-8500). In addition, PL decay curves in a ns range were also measured from 10 to 270 K using synchrotron radiation (SR) in a single-bunch mode with a beam energy of 750 MeV (BL3B line, UVSOR Facility, Institute for Molecular Science, Okazaki, Japan). Here, the SR pulse has an apparent duration of about 550 ps including the time response of the detection system, and the time interval between two consecutive SR pulses is about 177.6 ns [27]. The SR photons were dispersed by a 2.5-m off-plane Eagle-type monochromator set before the samples. Emitted PL photons were dispersed using many metal interference filters one by one, which also acted as filters to remove the excitation SR photons, and detected by a micro-channel plate photomultiplier tube (Hamamatsu Photonics).

Before and after the irradiation of photons with energies from 3.5 to 5.1 eV, ESR spectra were measured with JEOL JES-FA 300 at room temperature at 9.20 GHz (X band) using a microwave power of 5.00 mW. Here, the photons irradiated to samples were obtained by dispersing the light from a xenon lamp with a metal interference filter, and the number of photons that had reached the sample was estimated by taking account of the transmittance of the filter and the emission spectrum of the lamp. The irradiation time was determined so that the number of photons irradiated to each sample was set at a designated constant areal density of 1×10^{16} cm^{-2}. Furthermore, only the plate samples were used here, since ESR signals from the film samples were below the detection limit.

3 Results

Figure 1 shows in-plane XRD patterns observed in film samples obtained by spin-coating the YSZ solution containing 10 % of yttria once. Curves A, B, and C are patterns obtained for the films annealed at 300, 500, and 800 °C, respectively. The XRD pattern observed for the plate sample with 9.8 % of yttria is also shown (curve D). The film samples B and C annealed at temperatures higher than 500 °C show XRD peaks at $2\theta_\chi = 29.5°$, 34.5°, 49.1°, and 58.5°, which, respectively, correspond to the

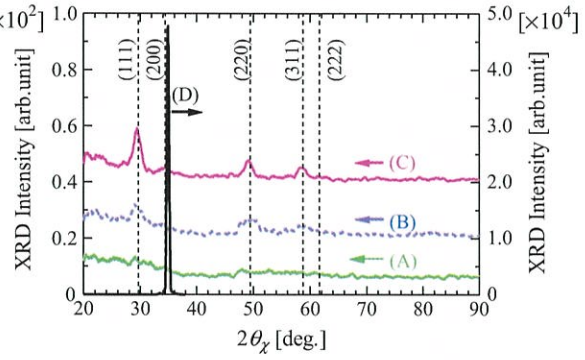

Fig. 1 XRD patterns observed in film samples annealed at 300 *(A)*, 500 *(B)*, and 800 *(C)* °C (*left ordinate*), and in the single crystal plate sample *(D)* (*right ordinate*). The three films contain yttria with a molar ratio of 10 %, while the plate contains 9.8 %. *Broken black vertical lines* represent typical diffraction angles ($2\theta_\chi$) characteristic to YSZ [28]

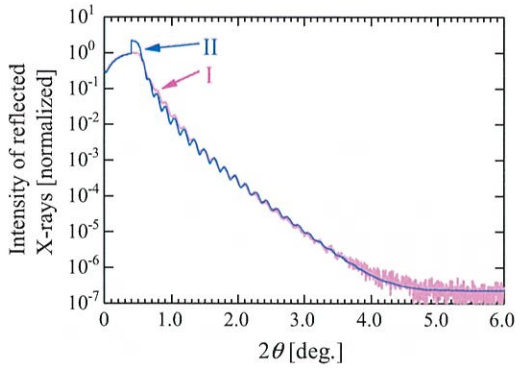

Fig. 2 Intensity of X-rays reflected on the surface of thin film sample as a function of grazing angle. The sample was annealed at 800 °C and is about 54 nm thick. It contains yttria with a molar ratio of 10 %. The *pink* (or I) and the *blue* (or II) *curves* represent the experimental result and simulation, respectively

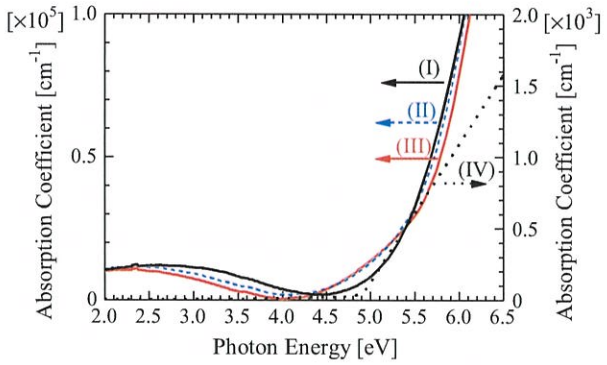

Fig. 3 Absorption spectra observed in film samples containing yttria with ratios of 10 *(I)*, 15 *(II)*, and 20 *(III)* mol% (*left ordinate*), and in the plate sample *(IV)* (*right ordinate*). The film samples were annealed at 800 °C and are about 162 nm thick

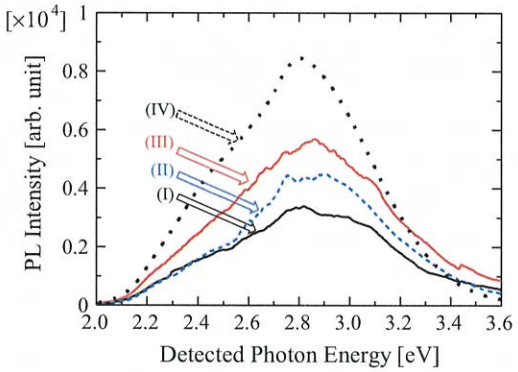

Fig. 4 PL spectra observed in film samples containing yttria with ratios of 10 *(I)*, 15 *(II)*, and 20 *(III)* mol%, and in the plate sample *(IV)*. The film samples were annealed at 800 °C and are about 162 nm thick. Note that the PL intensity can be compared among curves *(I)*–*(III)*, but not for curve *(IV)* obtained under a different condition

diffraction in (111), (200), (220), and (311) planes of YSZ [28]. This result indicates that these films are polycrystalline. On the other hand, the plate sample shows a single peak only at 34.9° due to the diffraction in the (200) plane. This is reasonable, since the sample had been set in a way that the (200) peak should have been observed.

Figure 2 shows reflectance of X-rays as a function of grazing angle, observed for the film sample spin-coated once and annealed at 800 °C. The intervals of peaks in reflectivity due to interference indicate that the thickness is about 54 nm. If the film thickness is in proportion to the number of spin-coating, the thickness is estimated to be about 162 nm for triple-coated films used for PL and optical absorption measurements. As mentioned above, films about one to several tens of micrometers are used for solid electrolytes in SOFCs and those about 0.1–1.0 μm are used for gate insulators in power MOSFETs. Therefore, the thickness of the present sample is similar to the latter and is suitable for this research that aims at clarifying the differences in the existing form of oxygen vacancy and its electronic excitation and relaxation processes between samples of a bulk shape and of a film shape.

Figure 3 compares optical absorption spectra among four samples with different thicknesses. Curves I, II, and III represent spectra measured for three film samples. Here, the films were obtained by spin-coating the YSZ solution containing yttria with the ratio of 10, 15, or 20 mol% three times. Then, the film on the substrate was annealed at 800 °C for 2 h. Curve IV represents the spectrum of the plate sample. The band-gap energy (E_g) was estimated by drawing the relation between $(\alpha h\upsilon)^{1/2}$ and $h\upsilon$, where α is the absorption coefficient and $h\upsilon$ is the photon energy. As a result, E_g is estimated to be around 4.9 eV for the plate sample. However, the estimation of E_g was difficult for the film samples, because a very broad peak stretching from a low energy to around 3.0 eV and a broad dip from around 4.0–5.0 eV appear seemingly due to interference. Nevertheless, E_g seems to be around 5.0 eV in all the three film samples, since the absorption becomes very large similarly to the plate sample.

Figure 4 shows PL spectra excited at around 5.5 eV for the same film and plate samples as those used for the absorption measurements. Note that the PL intensities can be compared only among the three film samples, because we had to widen the grating width of a monochromator in FP-8500 due to the weak PL in the film samples. Very broad PL with its peak at around 2.8 eV appears in all the samples. This PL is attributable to oxygen vacancies [24–26]. Furthermore, its intensity increases with the increase in yttria/zirconia ratio of the three film samples.

Figure 5 shows the PL excitation (PLE) spectra of the 2.8-eV PL observed in the film and plate samples. Here, the PLE spectrum means the spectrum showing the change in intensity of the corresponding PL (at 2.8 eV here) as a

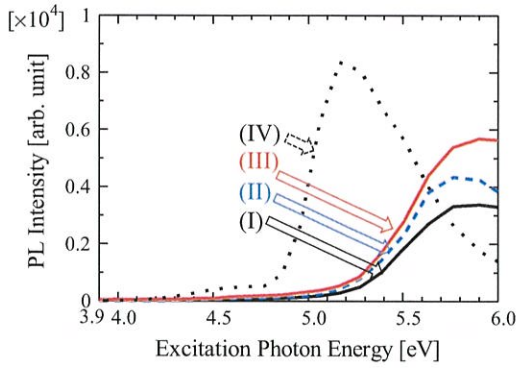

Fig. 5 PLE spectra of the 2.8-eV PL. The notations of curves are the same as those in Figs. 3 and 4

function of energy of incident excitation photons. The 2.8-eV PL appears when the energy of excitation photons reaches about 5.0 eV, although this threshold energy differs slightly between the plate sample and the three film samples.

Next, Fig. 6 shows decay profiles of the 2.8-eV PL observed in the film and plate samples, in a ns range measured at 10 K using SR photons (a) and in a ms range measured at 77 K using FP-8500 (b). It is indicated that the 2.8-eV PL has two decay time constants. Here, the SR pulse used for (a) has a triangular shape with an effective duration of about 550 ps [27], which is shorter than the ns-range time constant. By taking account of this duration, the shorter decay time constant is found to be 3.4 and 4.1 ns for the plate sample and the film sample, respectively. On the other hand, the excitation photons used for (b) show the decay that decreases almost exponentially as shown by solid blue triangles. Regarding this, the two decay curves denoted by open black circles and open red squares shown in (b) are convolutions of the decay of the excitation photons and the "true" decay of each PL. Therefore, by doing deconvolution [29], the longer decay time constant is found to be 0.38 ms for the plate sample and 0.40 ms for the film sample.

Similarly, Fig. 7 shows decay profiles of the 2.8-eV PL in the ns range measured at 10, 77, 130, 190, and 270 K. On the other hand, Fig. 8 shows those in the ms range measured at 77, 100, 130, 190, 230, and 270 K.

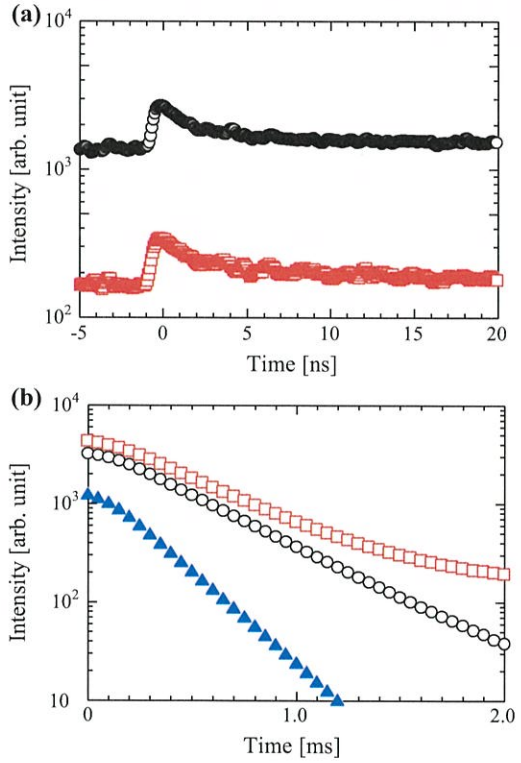

Fig. 6 Decay profiles of the 2.8-eV PL in a ns range (**a**) and in a ms range (**b**). *Open red* (*light gray* in b/w) *squares* and *open black circles* represent the profiles observed in the 162-nm-thick film sample with 10 mol% yttria annealed at 800 °C and the single crystal plate sample with 9.8 mol% yttria, respectively, while *solid blue* (*dark gray*) triangles represent the decay of the excitation photons from the measurement device (FP-8500)

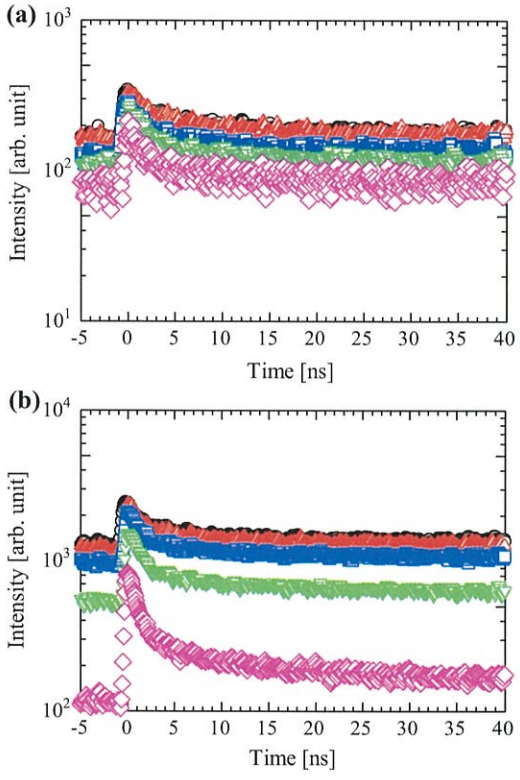

Fig. 7 Decay profiles of the 2.8-eV PL in a ns range measured at 10 (*black circles*), 77 (*red triangles*), 130 (*blue squares*), 190 (*light green inverted triangles*), and 270 (*pink diamonds*) K. **a** 162-nm film sample containing 10 mol% yttria annealed at 800 °C, **b** single crystal plate sample

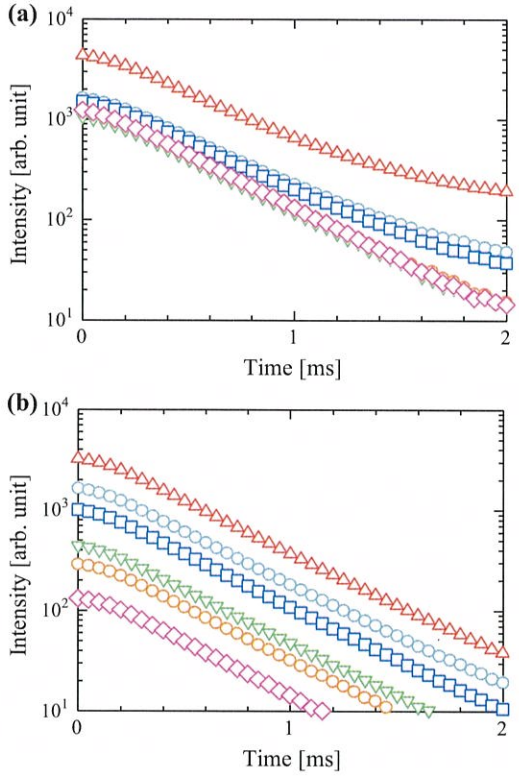

Fig. 8 Decay profiles of the 2.8-eV PL in a ms range measured at 77 (*red triangles*), 100 (*light blue circles*), 130 (*blue squares*), 190 (*light green inverted triangles*), 230 (*orange circles*), and 270 (*pink diamonds*) K. **a** 162-nm film sample containing 10 mol% yttria annealed at 800 °C, **b** single crystal plate sample. The PL intensity can be compared only in each figure

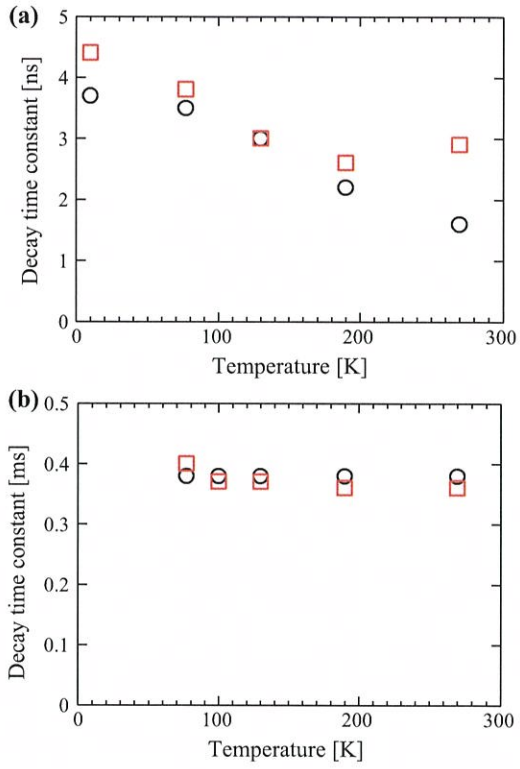

Fig. 9 Time constants of the 2.8-eV PL in the ns range (**a**) and in the ms range (**b**) as a function of measurement temperature, observed for the film sample with 10 mol% yttria [*red* (*gray* in b/w) *squares*] and for the single crystal plate sample with 9.8 mol% yttria (*black circles*)

Furthermore, Fig. 9 shows the two PL decay time constants in the ns and ms ranges as a function of the measurement temperature, calculated using data shown in Figs. 7 and 8. The shorter time constant becomes shorter with the increase in measurement temperature in both the film and plate samples, while the longer time constant hardly changes.

An oxygen vacancy in inorganic crystals such as oxides and aluminates is effectively equivalent to a positive divalent ion. Therefore, it is called F^{2+} center. When an oxygen vacancy captures one or two electrons, it becomes electrically positive monovalent or neutral, which is therefore called F^{+} or F center. Among the three types of oxygen vacancies, only the monovalent F^{+} center is ESR active.

Figure 10 shows ESR spectra measured for the plate sample, before and after the irradiation of 4.9-eV photons with an areal density of 1×10^{16} cm^{-2}. A signal is induced at around 336 mT ($g = 2.006$) by the irradiation, which seems to be due to the F^{+} centers [24, 25]. Here, the signal at 332 mT is due to a Mn marker used for calibrating the magnetic field and for quantifying the signal intensity.

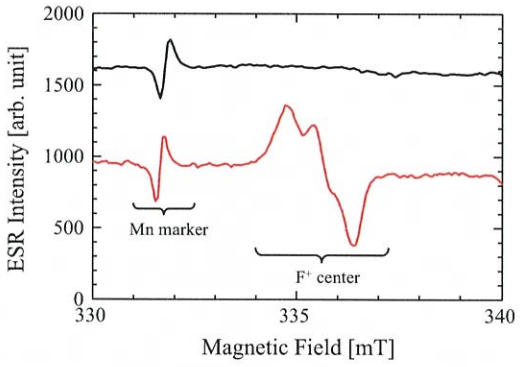

Fig. 10 ESR spectra observed for the single crystal plate sample with 9.8 mol% yttria, before and after the irradiation of 4.9-eV photons with an areal density of 1×10^{16} cm^{-2} from a xenon lamp. The signal at around 332 mT is due to a Mn marker used for calibrating the magnetic field and for quantifying the signal intensity

Next, UV photons with various energies were irradiated to the sample by adjusting the number of photons to the above-mentioned constant areal density of 1×10^{16} cm^{-2}. Figure 11 shows the intensity of the ESR signal due to the F^{+} centers induced in the plate sample as a function of energy of the irradiated photons. Here, when the sample was kept in the dark, the ESR signal soon disappeared.

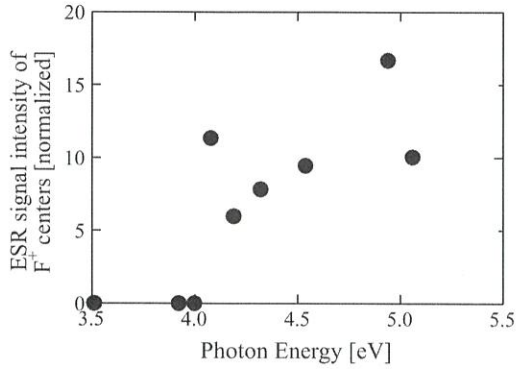

Fig. 11 ESR signal intensity, normalized by that of the Mn marker, due to F^+ centers observed for single crystal plate samples with 9.8 mol% yttria as a function of energy of irradiated photons

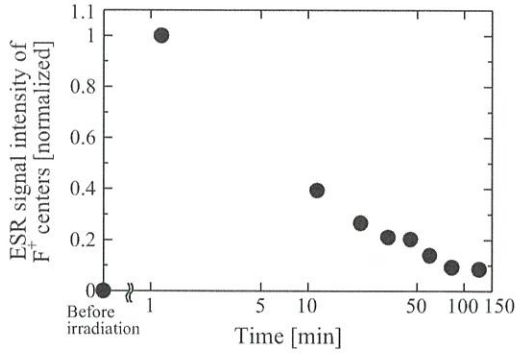

Fig. 12 Decay profile of the ESR signal intensity due to F^+ centers, induced by the irradiation of 5.6-eV photons in the single crystal plate sample with 9.8 mol% yttria. The measurements were done at room temperature before and after the photon irradiation. The abscissa represents the time after the cease of the irradiation. The intensity was normalized by its maximum value, observed 1 min after the cease of the irradiation

Therefore, only one sample was used throughout the repeated experiments done to take the data shown in Fig. 11. Figure 11 indicates that the F^+ centers appear when the energy of photons exceeds 4.0 eV.

Figure 12 shows how the ESR signal due to the F^+ centers, induced in the plate sample by the irradiation of 5.6-eV photons for 30 min, decays at room temperature as a function of time after the irradiation. It decreases to about $1/e$ in about 10 min. Note that no ESR signal could be detected in the film samples probably because they were too thin.

4 Discussion

As mentioned in relation to Eq. (1), YSZ crystal has abundant oxygen vacancies. Namely, oxygen vacancies appear in YSZ in proportion to the ratio of yttria incorporated into zirconia [1, 2]. Therefore, the abundance of oxygen vacancies in the film samples containing 10, 15, and 20 mol% of yttria should be 1.0:1.5:2.0. On the other hand, the ratios of the peak areas of the 2.8-eV PL shown in Fig. 4 are about 1.0:1.3:1.7 among these film samples, which are close to their abundance ratios of oxygen vacancies. Therefore, it is reasonable to consider that this PL originates in oxygen vacancies.

Next, we focus on the charging state of oxygen vacancies. As mentioned in relation to Fig. 6, the lifetime of the 2.8-eV PL has two decay components, namely the shorter time constant in the ns range and the longer one in the ms range. As for the PL component with the shorter time constant, it has been reported that the F^+ center in alumina brings about PL, which decays in a ns range ($\sim$2.1 ns) [30]. This is also the case in yttrium aluminate. Namely, yttrium aluminate exhibits PL with a time constant of about 2.7 ns due to the F^+ center [31]. Furthermore, it has been reported that potassium chloride, potassium fluoride, or sodium fluoride exhibits PL due to an anion vacancy that captures one electron, and that the decay time constant of each PL in a ns range becomes smaller with an increase in measurement temperature [32]. This temperature dependence of PL decay time constant is similar to that of the PL component with the shorter time constant observed in the present samples shown in Fig. 9a. These results indicate that the faster component of 2.8-eV PL in YSZ is ascribable to the F^+ center.

On the other hand, as for the PL component with the longer time constant, PL with a time constant of several milliseconds ($\sim$36 or 30 ms) observed in alumina or yttrium aluminate has been ascribed to the F center [30, 31]. Furthermore, the above PL in alumina hardly changes its decay time constant up to 400 K [33]. This temperature dependence is similar to that of the slower decay component of the 2.8-eV PL shown in Fig. 9b, indicating that the slower component seems to be due to the F center.

The above-mentioned presence of two decay time constants shown in Fig. 6 and their difference in temperature dependence shown in Figs. 7 to 9 indicate that the 2.8-eV PL surely originates from two kinds of oxygen vacancies, namely the F^+ and F centers. However, it is not so reasonable to assume that both the F^+ and F centers with different charging states emit photons with the same energy. As has already been reported for alumina [34], oxygen vacancies in YSZ tend to take the form of the F center, since it is the stablest neutral form. It has been reported that the F center in alumina becomes the F^+ center by releasing one electron when the sample is irradiated by UV photons [34].

The ESR results shown in Figs. 10, 11 and 12 clearly demonstrate that the F center is also the stablest in YSZ and that it becomes the F^+ center when it is irradiated by UV

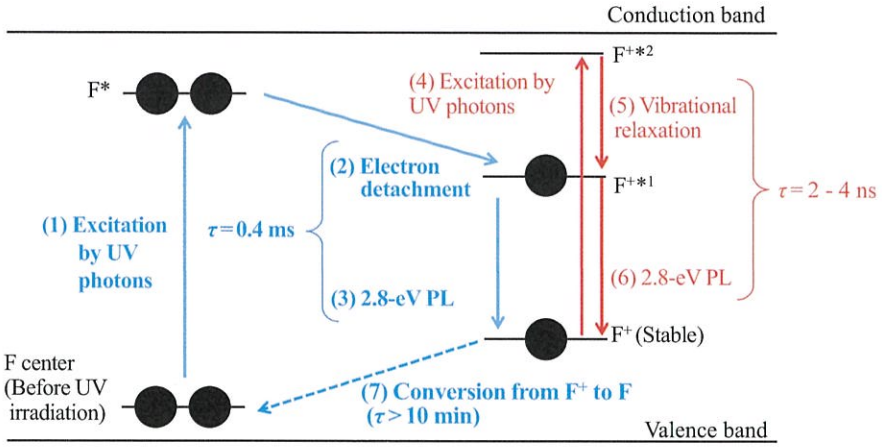

Fig. 13 Proposed processes of photo-induced electronic excitation of oxygen vacancy in YSZ and its relaxation accompanied by the 2.8-eV PL. *Asterisk marks* indicate excited states of the F and F^+ centers. The mutual relations of energy among the energy states of defects and the edges of the conduction and the valence bands are not within the scope of this figure, and they may differ slightly

photons. Note that neither F center nor F^{2+} center is detectable by ESR, since the two centers have no unpaired electrons. Figure 11 clearly indicates that the F^+ centers are induced when photons with energies higher than 4.0 eV are irradiated. An important fact is that this energy threshold is very similar to the onset energy of the PLE spectrum of the 2.8-eV PL shown in Fig. 5. Furthermore, as shown in Fig. 12, it takes a fairly long time for the F^+ centers, induced by the photon irradiation, to return back to the F centers.

Based on these facts, the model shown in Fig. 13 is proposed as the excitation and relaxation processes of oxygen vacancies in YSZ. Before the PL measurement or the photon irradiation, oxygen vacancies take the form of the stablest F center. When photons are irradiated, the F centers are excited as indicated by (1) in Fig. 13. Then, each excited F center releases one electron and becomes excited F^+ center as indicated by (2). Next, the excited F^+ centers emit photons during their relaxation process (3). If the process (2) is slow, phosphorescence appears. This seems to be observed as the slower decay component of the 2.8-eV PL. Since the F^+ centers are very stable compared to the repetition time intervals of 178 ns of the excitation SR pulses, they are excited directly to induce fluorescence with the time constant in the ns range through the processes (4)–(6).

5 Conclusions

The excitation and relaxation processes of oxygen vacancies in YSZ were studied experimentally, mainly focusing on the PL relevant to the vacancies and its decay. Important findings obtained using two types of samples with significantly different thicknesses are summarized as follows:

1. Crystalline YSZ has oxygen vacancies inherently in its crystal structure, regardless of its thickness whether it is as thick as 0.5 mm or as thin as around 160 nm. At the stablest state, oxygen vacancies tend to take the form of a neutral F center by capturing two electrons. When UV photons are irradiated to YSZ, the F centers release one electron each and become F^+ centers. The induced F^+ centers return back to F centers in about 10 min after the termination of photon irradiation.
2. The PL at 2.8 eV in YSZ is due to positive monovalent oxygen vacancy (F^+) centers. It has two components: one decays with a time constant of about 3–4 ns and the other decays in about 0.4 ms. It is highly probable that the faster decay appears when the F^+ centers are excited directly. On the other hand, the decay is observed in the ms range when the PL is induced by exciting neutral F centers, which follows the conversion to the F^+ centers by releasing electrons and the occurrence of the PL.

Acknowledgments This research was partly conducted in the UVSOR Facility, Institute for Molecular Science, Okazaki, Japan. It was partly supported by JSPS (Japan Society for the Promotion of Science) Grant 25 3090 for JSPS Fellows.

References

1. J.M. Costantini, F. Beuneu, W.J. Weber, J. Nucl. Mater. **440**, 508 (2013)
2. K.C. Lau, B.I. Dunlap, J. Phys. Condens. Matter **23**, 035401 (2011)
3. C. León, M.L. Lucía, J. Santamaría, Phys. Rev. **55**, 882 (1997)
4. C. Brahim, A. Ringuedé, E. Gourba, M. Cassir, A. Billard, P. Briois, J. Power Sources **156**, 45 (2006)
5. S. de Souza, S.J. Visco, L.C. De Jonghe, Solid State Ion. **98**, 57 (1997)
6. J. Zhu, Z.G. Liu, Mater. Lett. **57**, 4297 (2003)
7. Steven Sapp: U.S. Patent 6710403 B2 (2004)
8. Q. Zhang, M. Gomez, C. Bui, E. Hanna, in *Proceedings of International Symposium Power Semiconductor Devices and ICs 211* (2005)
9. K. Kanai, E. Hirata, Y. Ohki, Jpn. J. Appl. Phys. **47**, 7980 (2008)

10. E. Hirata, K. Tamagawa, Y. Ohki, Jpn. J. Appl. Phys. **49**, 091102-1 (2010)
11. H. Nishikawa, R. Tohmon, Y. Ohki, K. Nagasawa, Y. Hama, J. Appl. Phys. **65**, 4672 (1989)
12. H. Nishikawa, T. Shiroyama, R. Nakamura, Y. Ohki, K. Nagasawa, Y. Hama, Phys. Rev. B **45**, 586 (1992)
13. H. Nishikawa, R. Nakamura, Y. Ohki, Y. Hama, Phys. Rev. B **48**, 15584 (1993)
14. H. Kato, N. Kashio, Y. Ohki, K.S. Seol, T. Noma, J. Appl. Phys. **93**, 239 (2003)
15. K.S. Seol, T. Watanabe, M. Fujimaki, H. Kato, Y. Ohki, M. Takiyama, Phys. Rev. B **62**, 1532 (2000)
16. S. Munekuni, T. Yamanaka, Y. Shimogaichi, R. Tohmon, Y. Ohki, K. Nagasawa, Y. Hama, J. Appl. Phys. **68**, 1212 (1990)
17. S. Munekuni, N. Dohguchi, H. Nishikawa, Y. Ohki, K. Nagasawa, Y. Hama, J. Appl. Phys. **70**, 5054 (1991)
18. K.S. Seol, T. Futami, T. Watanabe, Y. Ohki, M. Takiyama, J. Appl. Phys. **85**, 6746 (1999)
19. K.S. Seol, A. Ieki, Y. Ohki, H. Nishikawa, M. Tachimori, J. Appl. Phys. **79**, 412 (1996)
20. H. Kato, A. Masuzawa, H. Sato, T. Noma, K.S. Seol, M. Fujimaki, Y. Ohki, J. Appl. Phys. **90**, 2216 (2001)
21. D. Yamasaka, K. Tamagawa, Y. Ohki, J. Appl. Phys. **110**, 074103-1 (2011)
22. M. Harima, T. Morimoto, Y. Ohki, IEEJ Trans. Electr. Electron. Eng. A **11**, 5 (2016)
23. T. Morimoto, M. Harima, Y. Horii, Y. Ohki, Nucl. Instrum. Methods B **366**, 198 (2016)
24. S. Kaneko, T. Morimoto, Y. Ohki, Jpn. J. Appl. Phys. **54**, 06GC03-1 (2015)
25. T. Morimoto, M. Takase, T. Ito, H. Kato, Y. Ohki, Jpn. J. Appl. Phys. **47**, 6858 (2008)
26. T. Morimoto, Y. Horii, T. Inoue, S. Kaneko, M. Harima, Y. Ohki, J. Inst. Eng. Electr. Disch. Jpn. **57**, 3 (2014). **(in Japanese)**
27. K. Kan'no, K. Tanaka, T. Mukai, Y. Nakai, M. Itoh, T. Miyanaga, K. Fukui, M. Watanabe, Phys. Scr. **41**, 120 (1990)
28. The International Centre for Diffraction Data (ICDD) PDF No. 01-077-2113
29. D.V. O'Connor, D. Philips, *Time-Correlated Single Photon Counting* (Academic Press, London, 1984), p. 164
30. A.I. Surdo, V.S. Kortov, V.A. Pustovarov, Radiat. Meas. **33**, 587 (2001)
31. Y.V. Zorenko, A.S. Voloshinovskiĭ, I.V. Konstankevych, Opt. Spectrosc. **96**, 532 (2004)
32. L.F. Stiles Jr., M.P. Fontana, D.B. Fitchen, Phys. Rev. B **2**, 2077 (1970)
33. M.S. Akselrod, N.A. Larsen, V. Whitley, S.W.S. McKeever, J. Appl. Phys. **84**, 3364 (1998)
34. K.H. Lee, J.H. Crawford Jr., Phys. Rev. B **19**, 3217 (1979)